

X-ray flares from dense shells formed in gamma-ray burst explosions

R. Hascoët^{1*}, A. M. Beloborodov¹, F. Daigne², R. Mochkovitch²

¹Physics Department and Columbia Astrophysics Laboratory, Columbia University, 538 West 120th Street, New York, NY 10027, USA.

²UPMC-CNRS, UMR7095, Institut d'Astrophysique de Paris, F-75014, Paris, France.

Accepted **.*.*. Received **.*.*.; in original form **.*.*.

ABSTRACT

Bright X-ray flares are routinely detected by the *Swift* satellite during the early afterglow of gamma-ray bursts, when the explosion ejecta drives a blast wave into the external medium. We suggest that the flares are produced as the reverse shock propagates into the tail of the ejecta. The ejecta is expected to contain a few dense shells formed at an earlier stage of the explosion. We show an example of how such dense shells form and describe how the reverse shock interacts with them. A new reflected shock is generated in this interaction, which produces a short-lived X-ray flare. The model provides a natural explanation for the main observed features of the X-ray flares — the fast rise, the steep power-law decline, and the characteristic peak duration $\Delta t/t = (0.1 - 0.3)$.

Key words: Gamma rays bursts: general; Radiation mechanisms: non-thermal; Shock waves.

1 INTRODUCTION

About 30% of GRBs show X-ray flares during their early afterglow (e.g. Burrows et al. 2005b; Falcone et al. 2007; Chincarini et al. 2010). Sometimes they are accompanied by significant flux increase in the optical band (e.g. Li et al. 2012). The X-ray flares are characterized by a fast rise of luminosity (typically by a factor ~ 10) to a sharp peak followed by a power-law decay (Chincarini et al. 2007). The ratio of the characteristic temporal width of the peak Δt_f to its time of occurrence since the beginning of the GRB is typically $\Delta t_f/t_f \sim 0.1 - 0.3$. At the end of the flare, the X-ray flux resumes the underlying smooth decay of the early afterglow, with no apparent flux increment left.

Besides the X-ray flares, the early afterglow shows other puzzling features, such as plateaus and sudden steep decrease in the observed luminosity. These features are not explained by the standard forward shock model (Meszaros & Rees 1997; Sari et al. 1998), and it was proposed that the observed afterglow is produced by a long-lived reverse shock inside the GRB ejecta (Uhm & Beloborodov 2007; Genet et al. 2007). The dynamics and emission of the reverse shock are particularly sensitive to the structure of the ejecta (the distribution of its Lorentz factor, density, and magnetic fields) which may explain the rich phenomenology of the early afterglow (Hascoët et al. 2011, 2012; Uhm et al. 2012; Hascoët et al. 2014b).

The fast rise and relatively short duration of the X-ray flares motivated several authors to invoke late activity of the central engine and associate the flares with the jet produced by this activity — a scaled-down version of the prompt GRB emission (e.g.

Burrows et al. 2005a; Fan & Wei 2005; Zhang et al. 2006). This possibility requires a mechanism that keeps the central engine active for about one day, as some flares are observed as late as a day after the GRB explosion. It also requires the engine to be variable in a special way on a timescale $\Delta t_f \sim (0.1 - 0.3)t_f$, in contrast to the much faster, multi-peak variability observed during the prompt GRB.

This Letter proposes an alternative possibility that the flares are produced by the long-lived reverse shock when it crosses the tail of the GRB ejecta. Our model does not require a long-lived central engine; it requires that the Lorentz factor in the end of the GRB explosion is significantly reduced, from $\Gamma \sim 100$ to $\Gamma \sim 10$, which leads to the formation of an extended tail (e.g. Uhm & Beloborodov 2007; Genet et al. 2007). As described in Section 2, dense shells are expected to form in the tail of the expanding ejecta before the passage of the reverse shock. In Section 3 we estimate the bolometric light-curve of emission produced by the encounter of the reverse shock with the dense shell, and find that it resembles the observed X-ray flares. Comparison of the model with observations and future possible ways of its development are discussed in Section 5.

2 DENSE SHELLS AFTER INTERNAL SHOCKS

The observed variability of GRB emission (Fishman & Meegan 1995; Beloborodov et al. 2000; Guidorzi et al. 2012) suggests that the Lorentz factor of the relativistic ejecta Γ fluctuates in a broad range of timescales, from a few milliseconds to several minutes. In the expanding outflow, regions where the radial gradient of Lorentz factor is negative (i.e. where Γ is decreasing outwards) are progressively compressed. If the ejecta is not magnet-

* E-mail: hascoet@astro.columbia.edu

ically dominated, internal shocks eventually form and propagate. The internal shocks can impact the prompt γ -ray emission mainly in two ways: (i) in the subphotospheric (optically thick) region, shock heating can offset the adiabatic cooling of radiation and change its spectrum from thermal to the observed Band-type shape through the Comptonization process and additional synchrotron emission (Mészáros & Rees 2000; Pe’er et al. 2006; Beloborodov 2010; Vurm et al. 2011); (ii) outside the photosphere, shocks can continue to produce synchrotron emission in the gamma-ray band if they efficiently accelerate particles (Rees & Meszaros 1994; Kobayashi et al. 1997; Daigne & Mochkovitch 1998).

The outflow is likely initially inhomogeneous, and internal shocks can amplify the density variations, especially if the shocks are radiatively efficient. More importantly, the outflow tends to develop a few massive dense shells long *after* the shocks. At time t_0 when the internal shock phase ends, the fluctuations of Lorentz factor Γ have been damped and Γ acquires a monotonic radial profile. Its slope $d\Gamma/dr > 0$ is significantly inhomogeneous, as illustrated below by a hydrodynamical simulation. The subsequent ballistic expansion of the outflow at $t \gg t_0$ generates a large contrast in density, as can be seen from the following estimate.

Consider a shell of width Δ_{sh} with the Lorentz factor variation across the shell $\delta\Gamma = (d\Gamma/dr)\Delta_{\text{sh}}$. As the shell expands ballistically, its width evolves as

$$\frac{\Delta_{\text{sh}}(t)}{\Delta_0} = 1 + \frac{\delta\Gamma}{\Gamma} \frac{t}{t_0}, \quad (1)$$

where Δ_0 is the shell width at t_0 . The relevant Δ_0 at the end of the internal shock phase corresponds to the longest variability timescale observed in the burst, $\Delta_0 \sim ct_0$, which is comparable to the burst duration, e.g. $t_0 \sim 1 - 10$ s. In contrast, the time t given to ballistic expansion before the reverse shock crosses the outflow in our model is associated with the observed time of the X-ray flares, $t \sim t_f \sim 10^3 - 10^4$ s.

The large ratio t/t_0 implies that $\delta\Gamma$ should strongly affect the density structure of the outflow. The parts of the outflow with $\delta\Gamma \sim \Gamma$ will become much thicker than the parts with $\delta\Gamma \ll \Gamma$, which will form dense shells. The corresponding density contrast is roughly given by

$$\frac{\rho_2}{\rho_1} \sim \min \left\{ \frac{\Gamma}{\delta\Gamma}, \frac{t}{t_0} \right\}. \quad (2)$$

An important feature of the post-internal-shock flows is the presence of a few “plateaus” in the profile of $\Gamma(r)$ or $\Gamma(m)$ where m is the Lagrangian mass coordinate in the flow. These plateaus contain a large mass and eventually form dense massive shells because of their small $\delta\Gamma$. We have observed and studied this effect in outflows with various initial $\Gamma(m)$ using detailed hydrodynamical simulations. We found that that the plateaus typically have a small $\delta\Gamma/\Gamma$ of a few per cent, even in the case of adiabatic shocks (an example is shown in Figure 1). The simulations have been performed using a one-dimensional (spherically symmetric) hydrodynamic code with a second-order HLLC approximate Riemann solver (Mignone & Bodo 2005) on a moving mesh (Duffell & MacFadyen 2011).

Similar (but exactly flat) plateaus are produced by simplified simulations in which the outflow is represented by a large number of discrete shells that interact by direct collisions (Daigne & Mochkovitch 1998). In this model, the ejecta is assumed to be cold and all pressure waves are neglected. This simplification is not crucial as it gives results similar to the detailed hydrodynamical simulations (cf. Daigne & Mochkovitch 2000). Below we

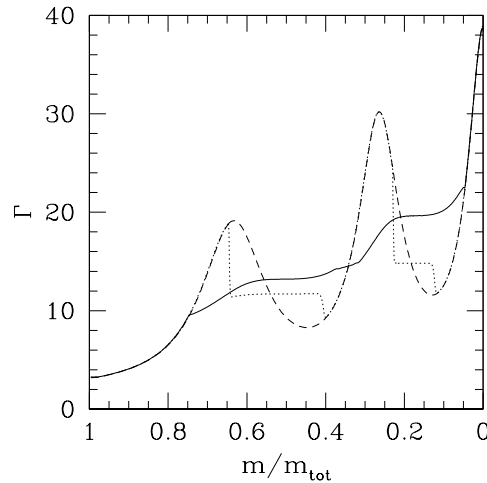


Figure 1. Hydrodynamic simulation of a spherical outflow undergoing internal shocks during its expansion. The flow is injected cold with a constant kinetic power during $t_w = 10$ s at a radius $R_0 = 0.1 ct_w$. The figure shows the Lorentz factor profile as a function of normalized Lagrangian mass coordinate, at three moments of time: the initial (injected) state (dashed line), during the internal shock phase at $t_{\text{lab}} = 800$ s (dotted line), and after internal shocks ended at $t_{\text{lab}} = 10^5$ s (solid line). At $t_{\text{lab}} = 10^5$ s, well after the internal shock phase, the outflow has cooled adiabatically and entered a ballistic phase. As a result of internal shocks, two large portions of the ejecta have a uniform Lorentz factor with $\delta\Gamma/\Gamma \lesssim 0.01$. We have checked that adding a fast variability component in the outflow (leading to several generations of internal shocks) does not significantly change the final Lorentz factor distribution.

use the simplified model and extend the simulation to include the external blast wave and the reverse shock propagation through the outflow.

3 FLARES: A SIMPLIFIED MODEL

We used the simplified hydrodynamical simulations to follow the reverse shock (RS) propagation through the outflow and its interaction with the dense shells. A sample model is shown in Figure 2. In this example, the explosion is assumed to produce an outflow of variable Lorentz factor distribution and duration $t_w = 10$ s. The injected kinetic power $\dot{E}_K = 10^{53}$ erg s^{-1} is assumed to be constant. Figure 2 shows how the initial distribution of Γ is changed after the internal shocks. Most of the outflow mass concentrates into three shells with Lorentz factors $\Gamma \approx 240$, 120 and 30 carrying about 10, 20, and 40 per cent of the total mass. The last 30 per cent of the outflow have not been affected by internal shocks.

We followed the outflow to much larger radii where the RS eventually crosses all three shells. The dynamics of the reverse shock depends on the external density. We have calculated two cases: a uniform external medium $\rho = \text{const}$ and a wind-like medium $\rho = Ar^{-2}$, where A is a constant which depends on the mass-loss rate of the GRB progenitor. Its typical range for galactic Wolf-Rayet stars is $10^{11} - 10^{12}$ g cm^{-1} (Crowther 2007). Recent modelling of optical and GeV flashes in GRBs suggest that $A \sim 10^{11}$ g cm^{-1} is typical for GRB progenitors (Hascoët et al. 2014a; Hascoët, Vurm & Beloborodov, to be submitted).

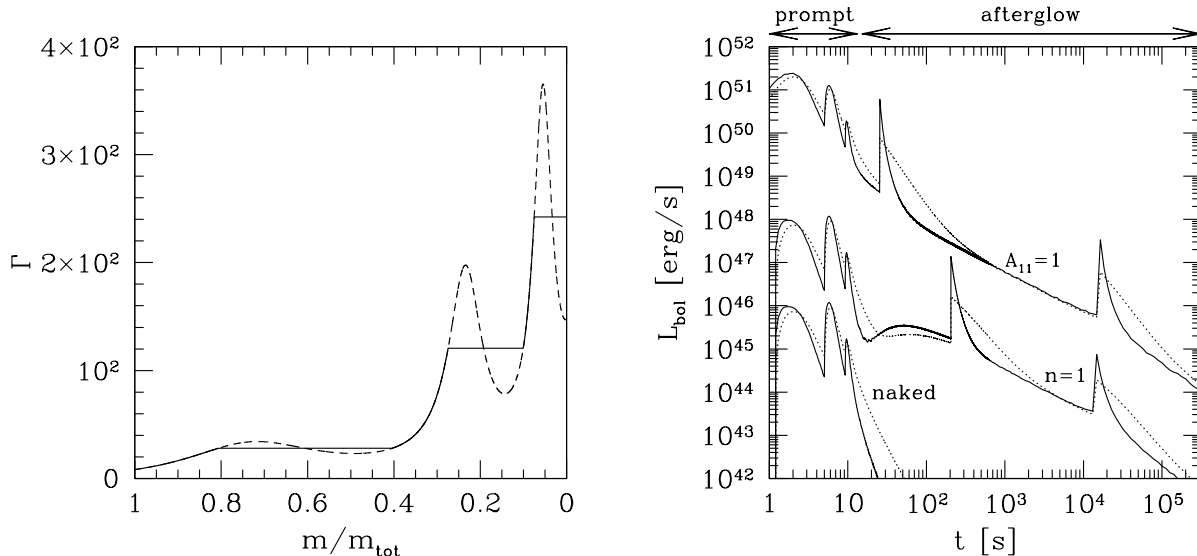


Figure 2. Left: Lorentz factor distribution as a function of Lagrangian mass coordinate; the front edge of the outflow is at $m = 0$. The initial distribution $\Gamma(m)$ is shown by the dashed curve, and the final distribution (after internal shocks) is shown by the solid curve. Right: bolometric light-curves (assuming a radiative efficiency $\epsilon_e = 0.1$) calculated for different ambient media (dotted lines). The wind density ρ is parametrized by A_{11} as follows: $\rho R^2 = 10^{11} A_{11} \text{ g cm}^{-1}$. In the uniform medium case, n is the density in cm^{-3} . From top to bottom: wind medium with $A_{11} = 1$, uniform medium with $n = 1$ (L_{bol} has been divided by 10^3), and the case of a “naked” burst (no ambient medium; L_{bol} has been divided by 10^5). The solid lines show the same light-curves for the case of an anisotropic emission, which is beamed within an angle $\theta_{\text{beam}} \approx 60^\circ$ in the plasma frame. In the case of the naked burst, the three early pulses (corresponding to the three pairs of internal shocks that initially propagate within the ejecta) are followed by high-latitude (off-axis) emission.

3.1 Bolometric light curve

The simulation gives the power dissipated in the RS and its bolometric luminosity with two assumptions: (i) that a fraction $\epsilon_e \sim 0.1$ of the dissipated energy is injected in shock-accelerated electrons, and (ii) that these electrons promptly radiate their energy (“fast-cooling” regime). To find the bolometric light curve received by a distant observer we transform the emission from the flow frame to the observer frame and take into account the spherical curvature of the emitting shells. The radiation received by the observer from the RS is shown in Figure 2. In this figure, we also included the prompt radiation produced by the internal shocks, assuming the same $\epsilon_e = 0.1$.

When the reverse shock goes through the dense shells there is a sudden rise of dissipated power producing a flare in the light curve. The immediate rise of luminosity to the peak of the flare in Figure 2 is an artefact of the simplified model, which does not resolve the propagation of the reverse shock through the dense shell. An accurate hydrodynamical model would give a slower but still a steep rise; it is discussed and estimated in Section 4 below.

In our example with three dense shells, two flares are produced; the crossing of the first shell (at $\Gamma \approx 240$) corresponds to the initial rise of dissipated power from the reverse shock. Using the approximate expression for the flare radius $R_f \sim \Gamma^2 c t_f$, one can estimate the observed time of the flare,

$$t_f = \left(\frac{3E}{4\pi n m_p c^3 \Gamma^8} \right)^{1/3} \approx 840 \left(\frac{E_{54}}{n} \right)^{1/3} \Gamma_2^{-8/3} \text{ s} \quad (\text{uniform}), \quad (3)$$

$$t_f = \frac{E}{4\pi A c^3 \Gamma^4} \approx 300 \left(\frac{E_{54}}{A_{11}} \right) \Gamma_2^{-4} \text{ s} \quad (\text{wind}). \quad (4)$$

Here Γ is the Lorentz factor of the massive shell ($\Gamma_2 = \Gamma/100$), E is

the kinetic energy of the ejecta that has already crossed the reverse shock ($E_{54} = E/10^{54} \text{ erg}$), n is the density of the uniform medium in cm^{-3} and A_{11} is the density parameter of the wind medium in units of $10^{11} \text{ g cm}^{-1}$. One can see that the flare can be significantly delayed and this delay is sensitive to the Lorentz factor of the massive shell.

We also observe that the flares produced by this mechanism share two key features with the observed X-ray flares: (i) after the flare the light curve returns to the pre-flare decaying afterglow and (ii) the flare duration Δt_f is proportional to its time of occurrence t_f .

The simulation shown in Figure 2 assumes fast cooling at all times, which gives a constant radiative efficiency equal to ϵ_e . The flux enhancement during the flare can be even higher if before and after the flare the emission is in the slow-cooling regime. Then the radiative efficiency can be significantly increased during the flare.

3.2 Effect of anisotropic emission

In the simplest model, which assumes isotropic emission in the fluid frame, the characteristic temporal width of the flare is $\Delta t_f \sim \tau$ where

$$\tau = \frac{R}{2\Gamma^2 c^2} \sim t_f. \quad (5)$$

Then the ratio $\Delta t_f/t_f$ is close to unity, greater than the typical observed ratio $\Delta t_f/t_f \sim 0.1 - 0.3$.

Significant anisotropy is, however, expected and supported by the fast luminosity variations observed in GRB afterglows (Beloborodov et al. 2011). The effect of anisotropy on the flare light curve is demonstrated by the following simple model.

For the moment, let us picture the encounter of the reverse shock with the dense shell as an instantaneous flash of energy E_f at a radius R . The bolometric light curve received from such a flash is given by (Beloborodov et al. 2011),

$$L(t) = \frac{2E_f A(\theta)}{\tau} \left(1 + \frac{t - t_f}{\tau}\right)^{-3} \quad (t > t_f), \quad (6)$$

where

$$\cos \theta = \frac{\tau - (t - t_f)}{\tau + (t - t_f)}, \quad (7)$$

θ is the angle with respect to the radial direction in the fluid frame, and $A(\theta)$ describes the angular distribution of emission; for isotropic emission $A(\theta) = 1$. The magnetic field in GRB shocks is in the shock plane, and their synchrotron radiation is anisotropic even when the emitting electrons are isotropic; in this case $A(\theta) = (3/4)(1 + \cos^2 \theta)$. Anisotropy of the electron distribution can further enhance the anisotropy of the emitted radiation, which significantly shortens the duration of the flare (see Figure 3 in Beloborodov et al. 2011), leading to a characteristic duration $\Delta t_f \ll t_f$. The shorter duration corresponds to a steeper decay of luminosity after the peak, with initial temporal index $\alpha \sim 3t_f/\Delta t_f$.

As an illustration, in Fig. 2 we show the model where the emission is moderately limb-darkened in the plasma frame, so that it is beamed within an angle $\theta_{\text{beam}} \approx 60^\circ$ (see Equation 9 in Beloborodov et al. 2011). Then $\Delta t_f \sim 0.3t_f$ and the resulting light curves resemble the observed X-ray flares.

4 SHOCK REFLECTION FROM THE DENSE SHELL

In the simplified model of Section 3, the RS crossing of the thin dense shell instantaneously dissipates part of the shell kinetic energy, and the observed light curve of the flash is determined by the curvature effect. In this section, we describe a more realistic picture of the RS interaction with the dense shell. We also estimate the timescales for the rise and duration of the dissipation event.

Two main effects should be taken into account: (i) The RS is greatly slowed down as it enters the dense gas, and it takes a finite time (estimated below) for the RS to cross the shell. (ii) The RS by itself does not efficiently decelerate the shell. The shell continues to plow through the ejecta that was previously accumulated in the blast wave. This ploughing launches a new internal shock inside the blast wave (Figure 3). Effectively, the RS splits in two when it enters the dense shell. One (slow) shock continues to propagate into the dense shell and the other (fast) shock is reflected and launched back into the blast wave material. The fast shock dissipates most of the kinetic energy of the massive shell measured in the rest-frame of the blast wave. Below we call it ‘internal forward shock’ (IFS). It is the IFS that emits the X-ray flare.

The velocity of RS propagation through the dense shell, $\beta_{\text{RS}} = v_{\text{RS}}/c \ll 1$, may be estimated using the approximate pressure balance between the RS and IFS. Let ρ_2 be the proper density of the shell just before it is reached by the RS. Assuming that the shell is cold and weakly magnetized, its pressure behind the RS jumps to

$$p_{\text{RS}} = \frac{3}{4} \beta_{\text{RS}}^2 \rho_2 c^2. \quad (8)$$

Now, let us estimate the pressure behind the IFS, p_{IFS} . The dense shell acts like a wall and the Lorentz factor downstream of the IFS is almost equal to the shell Lorentz factor Γ_{ej} . The relative Lorentz factor of the upstream and downstream is

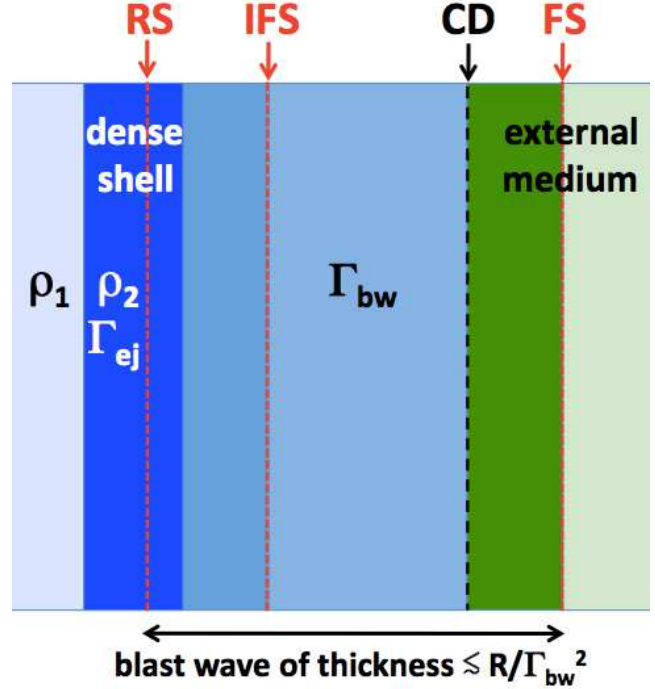


Figure 3. Schematic illustration of the reverse shock (RS) encounter with a thin massive shell. The RS becomes slow as it enters the dense material and a new ‘internal forward shock’ (IFS) is created, which propagates away from the dense shell into the blast wave material previously shocked by the RS. The figure also shows the forward shock (FS) in the external medium and the contact discontinuity (CD) that separates the ejecta from the external medium inside the blast wave.

$$\Gamma_{\text{rel}} = \frac{1}{2} \left(\frac{\Gamma_{\text{ej}}}{\Gamma_{\text{bw}}} + \frac{\Gamma_{\text{bw}}}{\Gamma_{\text{ej}}} \right), \quad (9)$$

where Γ_{bw} is the Lorentz factor of the blast-wave material upstream of the IFS, and we have used $\Gamma_{\text{ej}} \gg 1$ and $\Gamma_{\text{bw}} \gg 1$. Gas pressure may be written as $p \approx (\rho u/3)(1 + c^2/u)$ (Beloborodov & Uhm 2006), where ρ is the density and u is the energy per unit rest mass. The gas in the downstream of IFS has been shocked twice: first by the RS and then by the IFS, both times with the same relative Lorentz factor Γ_{rel} . Therefore, $u \approx \Gamma_{\text{rel}}^2 c^2$ and $\rho \approx (4\Gamma_{\text{rel}})^2 \rho_1$, where ρ_1 is the outflow proper density *prior to the crossing by the RS and IFS*. In the estimate for ρ we used the compression factor of $4\Gamma_{\text{rel}}$ for a strong adiabatic shock. This gives

$$p_{\text{IFS}} \approx \frac{16}{3} (\Gamma_{\text{rel}}^4 - 1) \rho_1 c^2. \quad (10)$$

The approximate pressure balance $p_{\text{RS}} \sim p_{\text{IFS}}$ gives an estimate for β_{RS} ,

$$\beta_{\text{RS}} \approx \frac{8}{3} \left[(\Gamma_{\text{rel}}^4 - 1) \frac{\rho_1}{\rho_2} \right]^{1/2}. \quad (11)$$

Using the obtained β_{RS} , we estimate the time it takes the RS to cross the dense shell, t_{cross} . The shell thickness is comparable to

$$\Delta_{\text{sh}} = \eta \left(\frac{\rho_1}{\rho_2} \right) \Delta_{\text{bw}}, \quad (12)$$

where $\Delta_{\text{bw}} \lesssim R/\Gamma_{\text{bw}}^2 \approx ct$ is the blast wave thickness, and $\eta = m_{\text{sh}}/m_{\text{bw}} \lesssim 1$ is the ratio between the mass of the incoming dense shell, m_{sh} , and the outflow mass already accumulated in the blast wave, m_{bw} . Then we find

$$t_{\text{cross}} \approx \frac{\Delta_{\text{sh}}}{2c\beta_{\text{RS}}} \lesssim 0.2\eta \left(\frac{\rho_1}{\rho_2}\right)^{1/2} (\Gamma_{\text{rel}}^4 - 1)^{-1/2} t. \quad (13)$$

Typical expected $\rho_2/\rho_1 > 30$ implies a short t_{cross} .

The shell Lorentz factor is reduced from Γ_{ej} to Γ_{bw} when it sweeps up the rest-mass

$$m_{\star} \sim \frac{m_{\text{sh}}}{\Gamma_{\text{rel}}^2}, \quad (14)$$

where we took into account that the gas ahead of the shell has been heated by the RS, and so its inertial mass is increased by the factor of Γ_{rel} . Assuming a relativistic IFS speed $\sim c$, this gives the following estimate for the observed duration of the shell deceleration:

$$t_{\text{diss}} \sim \frac{m_{\star}}{m_{\text{bw}}} \frac{\Delta_{\text{bw}}}{c} \left(\frac{\Gamma_{\text{bw}}}{\Gamma_{\text{ej}}}\right)^2 \lesssim \frac{m_{\star}}{m_{\text{bw}}} \left(\frac{\Gamma_{\text{bw}}}{\Gamma_{\text{ej}}}\right)^2 t. \quad (15)$$

The IFS may be mildly relativistic, $\Gamma_{\text{rel}} \sim 2$, if the flares occur long after the formation of the ballistic outflow ($t \gg t_0$). If the blast wave dynamics between the flares is approximated as self-similar, one finds $\Gamma_{\text{ej}}/\Gamma_{\text{bw}} = \sqrt{2}$ and 2 in the case of the wind and uniform external medium respectively.

The time t_{cross} is associated with the rise of the energy injection event and t_{diss} determines its duration. The above results give typical $t_{\text{cross}} \ll t_{\text{diss}} \ll t$. For short t_{diss} the observed duration of the flare will be determined by the curvature (and anisotropy) effects, as described in Section 3.2. Here we note an additional effect which reduces the observed duration of the flare. While the pre-flare afterglow is emitted by gas moving with Γ_{bw} , the flare is emitted by gas moving with $\Gamma_{\text{ej}} > \Gamma_{\text{bw}}$ (the gas behind the IFS). Therefore, even without the anisotropy effect, the curvature timescale for the flare is compressed by the factor of $\Delta t_f/t_f \sim (\Gamma_{\text{bw}}/\Gamma_{\text{ej}})^2$.

5 CONCLUSIONS

This Letter suggests that GRB outflows naturally develop a few dense shells with relatively low Lorentz factors, which leads to a new explanation for the X-ray flares. The dense shells give sudden energy injections to the GRB afterglow. We examined the dynamics of the injection event and showed that it generates a new internal shock behind the blast wave, which produces a short-lived flare. This mechanism provides a natural explanation for the fast rise of the X-ray flares and their observed duration $\Delta t_f/t_f \sim 0.1 - 0.3$.

The proposed scenario assumes two radiative properties of the shock: (i) a fraction of the shock energy is transferred to non-thermal accelerated electrons capable of emitting synchrotron X-rays, and (ii) the electrons radiate X-rays in the fast cooling regime. Detailed modeling of hydrodynamics and radiative properties of the flares are deferred to a future work. As described in Section 4, the flare is emitted by gas that has been shocked twice and has high density and pressure. This gas can also possess strong magnetic fields and can radiate more efficiently compared with the pre-flare afterglow. This will help to satisfy the conditions (i) and (ii).

ACKNOWLEDGMENTS

It is a pleasure to thank H. van Eerten and A. I. MacFadyen for useful discussions on hydrodynamics simulations. This work has been partially supported by the Programme National Hautes Energies (PNHE) and the French Space Agency (CNES). AMB was supported by NSF grant AST-1412485 and NASA Swift Cycle 10 grant NNX14AI94G.

REFERENCES

- Beloborodov, A. M. 2010, MNRAS, 407, 1033
 Beloborodov, A. M., Daigne, F., Mochkovitch, R., & Uhm, Z. L. 2011, MNRAS, 410, 2422
 Beloborodov, A. M., Stern, B. E., & Svensson, R. 2000, ApJ, 535, 158
 Beloborodov, A. M., & Uhm, Z. L. 2006, ApJL, 651, L1
 Burrows, D. N., Romano, P., Falcone, A., et al. 2005a, Science, 309, 1833
 Burrows, D. N., Hill, J. E., Nousek, J. A., et al. 2005b, Space Science Reviews, 120, 165
 Chincarini, G., Moretti, A., Romano, P., et al. 2007, ApJ, 671, 1903
 Chincarini, G., Mao, J., Margutti, R., et al. 2010, MNRAS, 406, 2113
 Crowther, P. A. 2007, Annual Review of Astronomy and Astrophysics, 45, 177
 Daigne, F., & Mochkovitch, R. 1998, MNRAS, 296, 275
 Duffell, P. C., & MacFadyen, A. I. 2011, ApJS, 197, 15
 Falcone, A. D., Morris, D., Racusin, J., et al. 2007, ApJ, 671, 1921
 Fan, Y. Z., & Wei, D. M. 2005, MNRAS, 364, L42
 Fishman, G. J., & Meegan, C. A. 1995, Annual Review of Astronomy and Astrophysics, 33, 415
 Genet, F., Daigne, F., & Mochkovitch, R. 2007, MNRAS, 381, 732
 Guidorzi, C., Margutti, R., Amati, L., et al. 2012, MNRAS, 422, 1785
 Hascoët, R., Beloborodov, A. M., Daigne, F., & Mochkovitch, R. 2014a, ApJ, 782, 5
 Hascoët, R., Daigne, F., & Mochkovitch, R. 2012, A&A, 541, A88
 —. 2014b, MNRAS, 442, 20
 Hascoët, R., Uhm, Z. L., Mochkovitch, R., & Daigne, F. 2011, A&A, 534, A104
 Kobayashi, S., Piran, T., & Sari, R. 1997, ApJ, 490, 92
 Li, L., Liang, E.-W., Tang, Q.-W., et al. 2012, ApJ, 758, 27
 Meszaros, P., & Rees, M. J. 1997, ApJ, 476, 232
 Mészáros, P., & Rees, M. J. 2000, ApJ, 530, 292
 Mignone, A., & Bodo, G. 2005, MNRAS, 364, 126
 Pe’er, A., Mészáros, P., & Rees, M. J. 2006, ApJ, 642, 995
 Rees, M. J., & Meszaros, P. 1994, ApJL, 430, L93
 Sari, R., Piran, T., & Narayan, R. 1998, ApJL, 497, L17
 Uhm, Z. L., & Beloborodov, A. M. 2007, ApJL, 665, L93
 Uhm, Z. L., Zhang, B., Hascoët, R., et al. 2012, ApJ, 761, 147
 Vurm, I., Beloborodov, A. M., & Poutanen, J. 2011, ApJ, 738, 77
 Zhang, B., Fan, Y. Z., Dyks, J., et al. 2006, ApJ, 642, 354